

Dried Blood Matrix as a New Material for the Detection of DNA Viruses

Jongwon Lim, Joanne Hwang, Hyegi Min, Matthew Wester, Chansong Kim, Enrique Valera, Hyun Joon Kong, and Rashid Bashir*

The gold standard for diagnosing viruses such as the Hepatitis B Virus has remained largely unchanged, relying on conventional methods involving extraction, purification, and polymerase chain reaction (PCR). This approach is hindered by limited availability, as it is time-consuming and requires highly trained personnel. Moreover, it suffers from low recovery rates of the nucleic acid molecules for samples with low copy numbers. To address the challenges of complex instrumentation and low recovery rate of DNA, a drying process coupled with thermal treatment of whole blood is employed, resulting in the creation of a dried blood matrix characterized by a porous structure with a high surface-to-volume ratio where it also inactivates the amplification inhibitors present in whole blood. Drawing on insights from Brunauer–Emmett–Teller (BET)- Barrett–Joyner–Halenda (BJH) analysis, scanning electron microscopy (SEM), and fluorescence recovery after photobleaching (FRAP), detection assay is devised for HBV, as a demonstration, from whole blood with high recovery of DNA and simplified instrumentation achieving a limit of detection (LOD) of 10 IU mL⁻¹. This assay can be completed in <1.5 h using a simple heater, can be applied to other DNA viruses, and is expected to be suitable for point-of-care, especially in low-resource settings.

1. Introduction

In vitro diagnostics in blood have been widely used for the accurate identification of disease-causing agents.^[1,2] To achieve accurate diagnostic outcomes, it is important to begin with highly purified target molecules such as proteins or nucleic acids. This ensures reliable results without significant interference or false positives.^[3,4] Therefore, the conventional diagnostic methodology from blood can be delineated in the following steps; a) the extraction of requisite target DNA from pathogens in the sample of interest; b) subsequent purification of desired target molecules amongst a multitude of contaminants and inhibitors in the bloodstream; c) transfer of the purified DNA into reagents designed for subsequent amplification processes such as PCR; and d) detection of the amplification signal.

Despite significant advancements in reagent technology and effective extraction of pathogenic DNA, including the development of isothermal amplifications such

J. Lim, H. Min, M. Wester, E. Valera, R. Bashir
Nick Holonyak Jr. Micro and Nanotechnology Laboratory
University of Illinois at Urbana–Champaign
Urbana, IL 61801, USA
E-mail: rbashir@illinois.edu

J. Lim, M. Wester, E. Valera, R. Bashir
Department of Bioengineering
University of Illinois at Urbana–Champaign
Urbana, IL 61801, USA

J. Lim, J. Hwang, H. J. Kong, R. Bashir
Carl R. Woese Institute for Genomic Biology
University of Illinois at Urbana–Champaign
Urbana, IL 61801, USA

J. Hwang, H. J. Kong
Department of Chemical and Biomolecular Engineering
University of Illinois at Urbana–Champaign
Urbana, IL 61801, USA

C. Kim, R. Bashir
Department of Materials Science and Engineering
University of Illinois at Urbana–Champaign
Urbana, IL 61801, USA

H. J. Kong
Departments of Pathobiology
University of Illinois at Urbana–Champaign
Urbana, IL 61801, USA

R. Bashir
Department of Mechanical Science and Engineering
University of Illinois at Urbana–Champaign
Urbana, IL 61801, USA

R. Bashir
Department of Biomedical and Translational Science
Carle Illinois College of Medicine
University of Illinois at Urbana–Champaign
Urbana, IL 61801, USA

R. Bashir
Chan Zuckerberg Biohub Chicago
Chicago, IL 60642, USA

 The ORCID identification number(s) for the author(s) of this article can be found under <https://doi.org/10.1002/adhm.202402506>

© 2024 The Author(s). Advanced Healthcare Materials published by Wiley-VCH GmbH. This is an open access article under the terms of the [Creative Commons Attribution-NonCommercial-NoDerivs License](#), which permits use and distribution in any medium, provided the original work is properly cited, the use is non-commercial and no modifications or adaptations are made.

DOI: 10.1002/adhm.202402506

as loop-mediated isothermal amplification (LAMP)^[5] or recombinase polymerase amplification (RPA),^[6] as well as the incorporation of glass disruptor bead for efficient bacterial rupture,^[7] existing diagnostic methodologies continue to face notable limitations. These limitations primarily stem from the restricted accessibility resulting from time-consuming extraction and purification procedures.^[8,9] In addition to the necessity for highly skilled personnel and the associated costs and time constraints, the multi-step protocol itself presents a fundamental challenge. For viruses, this protocol involves pathogen lysis using chemical buffers with thermal treatment, DNA precipitation through ethanol treatment, and removal of contaminants via the binding and unbinding of target DNA to silica or magnetic beads, followed by washing and elution steps. Each of these steps carries inherent risks of DNA loss and potential contamination, which can result in very low recovery rates of target DNA or the inclusion of unwanted impurities in subsequent steps. Consequently, despite the exceptional sensitivity of amplification methods, blood diagnostics frequently yield false-negative results due to an insufficient amount of starting material following the extraction and purification steps.^[10,11]

To tackle the challenges linked to diagnostics alongside extraction and purification processes, considerable efforts have been focused on directly detecting pathogens from crude samples.^[12,13] Blood presents one of the most formidable challenges in molecular biology and diagnostics due to its complex nature. For bacteria, the culture step is always added to grow the pathogens and adds to the time to result, up to 5 days for confirmed negative.^[2] For viruses, as culture is not a practical option in clinical labs, the only option is to detect it directly, thus increasing significantly the minimum detection concentrations.^[14] There have been relatively fewer studies exploring direct detection from blood specimens as compared to the detection of viruses from the nose.^[9,15] Another notable obstacle is the lower concentration of pathogens in blood as compared to for example respiratory panels, making detection considerably more difficult.^[16] For example, COVID or respiratory pathogens usually display concentrations ranging from 10 to 1000 copies in a few microliters of viral transport media or saliva.^[17] In scenarios involving sepsis or hepatitis infection, on the other hand, blood samples typically house only 1 to 10 pathogens per milliliter in the initial phases, leading to significantly diminished recovery rates during extraction and purification.^[18,19] Hence, the sensitivity of direct (without culture) pathogen detection methods from whole blood is severely restricted.

To address these challenges, we have reported a new method that we have called biphasic reaction, which involves directly introducing detection reagents into the dried blood matrix.^[20,21] This innovative approach diverges from the norm and provides a solution by reversing the diagnostic pathway, with a focus on delivering abundant reagents into samples with low concentrations of pathogens, rather than attempting to extract minute amounts of target DNA from complex matrices containing multiple inhibitors. The dried blood structure physically traps the inhibitors, confining them within the solid phase and obstructing their release into the liquid phase.^[21] Our research findings indicate that this biphasic approach can be coupled with diverse types of isothermal amplification, such as LAMP or RPA, resulting in high sensitivity.^[20,21]

Despite all the progress we have made in understanding our technology, there are still unanswered questions regarding the mechanisms underlying the formation process of the dried blood matrices, the characterization of the matrix from a material perspective, and the rate at which reagents can traverse through the porous structure. Another aspect that we have not yet explored is whether biphasic technology can also be used for virus detection. Hence in this study, we introduce the dried blood matrix as a novel material for diagnostic platforms for viruses. By characterizing the properties of the dried blood matrix, including pore size distribution and permeability, we expand the understanding of the material properties that are used to explain past results and can be used to design future assays. Through a series of investigations, we explored the surface characteristics of the matrix, quantified the distribution of pores within it, and examined the diffusion coefficient of molecules within its structure. Leveraging this foundational understanding, we have developed an assay for the direct detection of Hepatitis B Virus (HBV) from whole blood samples, bypassing the need for traditional extraction and purification steps. Our biphasic HBV detection method has exhibited superior sensitivity compared to the current state-of-the-art approach, which involves extraction, purification, and subsequent PCR reaction. By taking advantage of the unique properties of the dried blood matrix, we unlock new possibilities for rapid and highly sensitive diagnostic testing.

2. Results and Discussion

2.1. Concept of the Biphasic Reaction for Viral DNA Detection

The current gold standard technology for detecting hepatitis B virus is limited to centralized laboratories, mainly because of the instrumentation and the laborious process involved (Figure 1A–D).^[22,23] The process begins with centrifugation to isolate plasma from whole blood to reduce interference from cellular components (Figure 1B). Despite this, plasma still contains numerous contaminants, necessitating DNA extraction and purification (Figure 1C). The purified DNA is then transferred to an amplification master mix and loaded into PCR tubes for amplification using a PCR machine (Figure 1D). This overall process relies on complex instruments such as a centrifuge capable of speeds ≈ 2000 g, spin columns for purification, and a benchtop thermocycler for precise PCR temperature control. Another challenge associated with extraction and purification is that it requires hands-on processing by personnel with advanced training. While there are automated machines available for these steps, they significantly increase costs. Due to these constraints, these equipment and processes are only available in centralized labs, and sample transport to these laboratories can take several days. This potentially delays necessary medical interventions, particularly in remote locations (Figure 1A).^[24,25]

Our proposed approach termed biphasic assay, aims at overcoming the limitations of existing methodologies by directly incorporating reagents into dried blood samples.^[21] Our approach involves simple blood drying (Figure 1E) followed by an additional heating step for enhanced sensitivity (Figure 1F). Then, the master mix is added to the sample (Figure 1G), followed by isothermal amplification (Figure 1H). This streamlined procedure necessitates only a simple heater, requiring just under 15

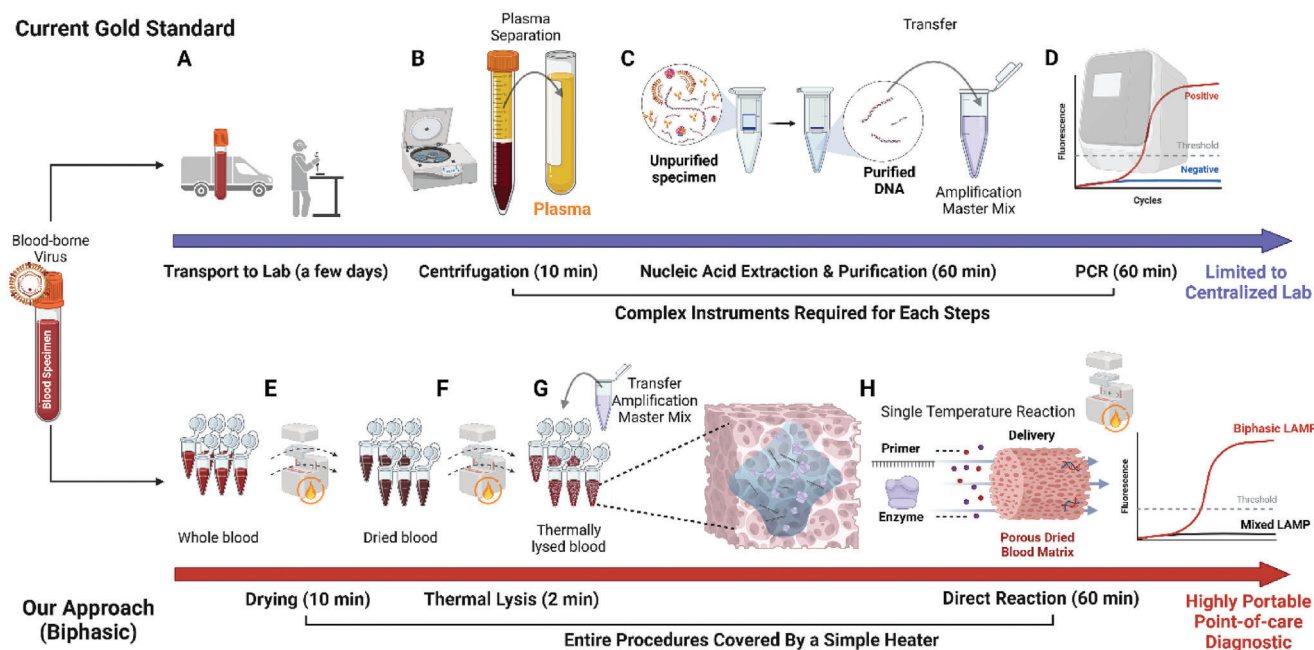


Figure 1. Comparison of two different HBV detection methods. A–D) Current gold standard methods use extraction and purification along with PCR. E–H) Biphasic methods for direct detection of DNA through blood drying process.

min for sample processing and an additional up to 60 min or less for amplification and detection. Importantly, our method eliminates the need for centrifugation and permits the use of whole blood as the starting material. Consequently, samples do not need to be transported to a centralized laboratory. To achieve this, we have concentrated on addressing the disparity between the concentration ranges of target DNA in specimens, ranging from attomolar (10^{-18}) to femtomolar (10^{-15}), and the reagents in the amplification master mix, which typically range from micromolar (10^{-6}) to millimolar (10^{-3}) concentrations (Figure S1, Supporting Information). This significant contrast underscores the importance of effectively delivering the master mix to the target DNA, considering we have an abundance of the latter.

2.2. Three Steps Underlying the “Biphasic” Assay Technology

Within our sample processing regimen, we employ two consecutive heating steps: a drying step (Figure 1E) and a thermal lysis step (Figure 1F). During each step, different underlying mechanisms occur advancing the biphasic reaction, eventually resulting in an increase in sensitivity as compared to the current state-of-the-art PCR method. The three steps uniquely tuned in our reactions are diffusion, immobilization, and reaction.

2.2.1. Diffusion

When adding whole blood directly to the reaction master mix (direct detection), inhibitors can freely attach to amplification components, causing non-specific binding and impeding the desired reaction (Figure S2A, Supporting Information).^[21] To prevent this, conventional diagnostic procedures typically commence

with purified DNA lacking inhibitor components to avert undesirable outcomes (Figure 1C). However, the low recovery rate remains a significant concern, primarily attributable to the inherent loss of DNA during the binding and unbinding process.^[11] Considering the diffusion mechanism, this situation presents molecular diagnostics with the dilemma of selecting between purified samples containing undetectable amounts of DNA or unpurified samples containing DNA without loss but alongside inhibitors and impurities.

2.2.2. Immobilization

Tuning the immobilization aspect can be a solution to this challenge. Either the fibrin structure or denatured proteins formed during the blood drying entrap inhibitor components within their matrix (Figure S2B, Supporting Information). This immobilization of the inhibitors prevents them from freely interacting with primers and enzymes, ensuring interference-free reactions. Firstly, our prior research showed that most amplification inhibitors, such as hemoglobin and immunoglobulin G, lose their inhibitory capacity post-blood drying.^[21] Nevertheless, the dried blood matrix initially lacks adequate porosity and matrix characteristics for efficient diffusion of the primers and enzymes.

2.2.3. Reaction and Increased Sensitivity

After the deactivation of inhibitors as noted above, the successful detection of DNA in dried blood relies on the efficient transport of enzymes or primers to the site of the target DNA, which is likely situated across the dried blood matrix (Figure S3D, Supporting Information). The additional heating step becomes imperative

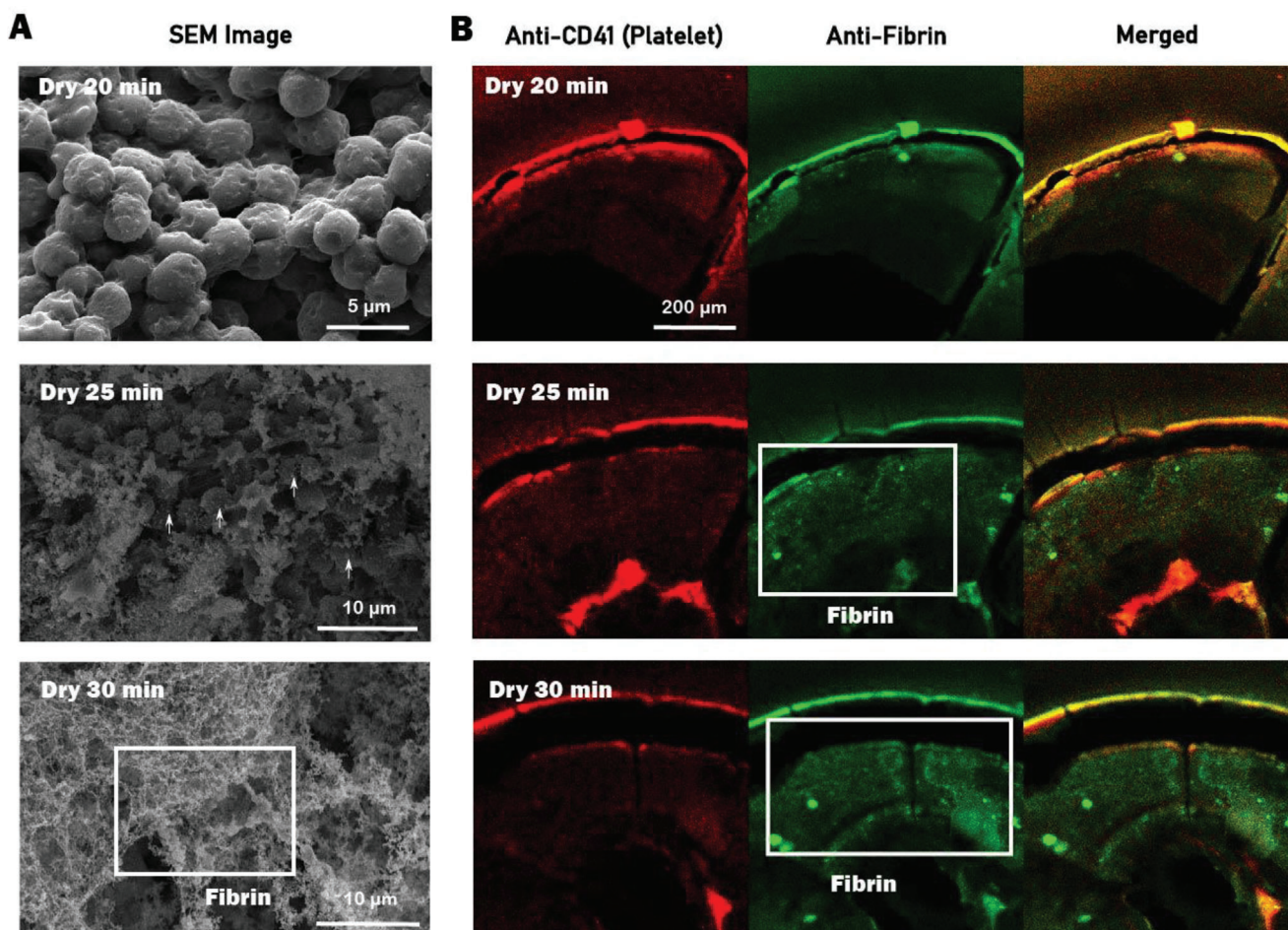


Figure 2. Characterization of SEM and Immunostaining of the dried blood matrix based on drying time. A) SEM image displaying the surface of the dried blood matrix after 20–30 min of drying time B) Immunostaining of the dried blood matrix illustrating the progression of the fibrin structure with respect to the drying time. The immobilization aspect was achieved based on these fibrin structures.

to ensure that this reaction can occur (Figure S2C, Supporting Information). The process of adding buffer mix to dried blood and incubating at 95 °C for 2 min results in increased porosity while preserving inhibitor deactivation. The elevated thermal energy generated at high temperatures prompts water molecules to traverse through the minute pores within the dried blood matrix, thereby increasing the matrix's surface area and porosity. With increased porosity, primers and enzymes can travel further and faster within the matrix.

2.3. Imaging of the Dried Blood Structures through SEM

In Figure 2, the process of achieving immobilization through blood drying is depicted. Our investigation into the surface morphology of the dried blood matrix using SEM facilitated visual examination of surface topography, alongside a detailed assessment of size, shape, and distribution. Analysis of the SEM image revealed spherical features on the matrix surface (Figure 2A), which were surrounded by numerous empty spaces. Intrigued by the potential presence of pores within the inner layer, we subjected the matrix to fracturing and conducted further SEM analysis. Re-

markably, similar spherical features were observed within the inner layer (Figure S4, Supporting Information), suggesting that the interior is not simply a dense, solid structure, but also harbors void spaces or pores through which enzymes and primers can traverse.

As shown in Figure 2, fibrin structures are created during the blood-drying process. First, the Scanning electron microscope (SEM) images show that drying induces the formation of spherical features on the surface, with smaller granules (pointed with arrows) present on these features (Figure 2A; Figure S5, Supporting Information). Considering the substantial presence of these attributes within the structure and their morphology, it is hypothesized that the larger spherical features represent red blood cells (RBCs, Figure S6, Supporting Information). Despite their size not aligning with the standard diameter of RBCs (6–8 μm), the elimination of moisture and dehydration during the drying processes might lead to a reduction in cell size. Regarding the smaller granules observed on the RBCs, prior investigations have noted similar phenomena during RBC stimulation through Ca^{2+} uptake, resulting in RBC-derived microvesicles. However, there is no current report suggesting that these granules can be generated during the blood-drying process. While it is conceivable for

RBCs to lose water during drying, which may lead to cell membrane reorganization, membrane blebbing, and microvesicle formation, further validation is required to confirm this. Notably, an intriguing characteristic is observed with extended drying periods, where the number of granules or smaller blebbing particles increases, eventually forming interconnected spiderweb-like or silk-like structures. Upon closer examination, these web structures consist of numerous smaller-sized granules and interconnections (Figures S7 and S8, Supporting Information).

2.4. Confocal Imaging of Fibrin Formation During Blood Drying

Confocal microscopy examination of immunocytochemistry data provides evidence supporting the identification of these formations as fibrin structures in Figure 2B. Blood samples subjected to varying durations of drying were individually stained with anti-CD41 and anti-Fibrin antibodies. The anti-CD41 staining revealed the distribution of platelet molecules, with red fluorescence observed throughout the dried blood matrix structure (Figure 2B).^[26] Notably, discernible concentrations of fibrin structures were absent until the 20-minute mark, thereafter, exhibiting numerous small green fluorescence spots consistent with fibrin structure after 25 min. Merged images from both channels illustrated both the background signal and the fibrin-specific signal evident in the 25- and 30-minute images. Fibrin structures are well-known for their crucial role in blood clotting or coagulation. This process produces insoluble fibrin strands, enhancing the structural stability of the dried blood matrix by making the clot resistant to dissolution in liquid. Additionally, coagulation-based clots physically trap amplification inhibitors through polymerization, where fibrin molecules bind together to form long, insoluble strands. These strands can cross-link to create a mesh-like structure, the foundation of a blood clot, effectively immobilizing inhibitors and preventing their free movement. Therefore, adequate drying time is crucial to provide structural stability for biphasic formation. However, as noted in our previous publication, excessive drying time may cause the dried blood matrix to separate from PCR tubes and float, contributing to signal interference.^[20]

2.5. Analysis of Pore Size Distribution

In Figures 3 and 4, the enhanced sensitivity via additional thermal lysis is demonstrated. Figure 3 shows SEM and BET and BJH analysis to explore the distribution of pore sizes that allow reagents to diffuse through the matrix. Previously, we demonstrated that incorporating an additional thermal lysis step following blood drying leads to enhanced sensitivity. Following thermal lysis as a secondary heating step, the features located at the surface exhibit a considerable reduction in size, with an increased number of smaller features (Figure 3A,B), from $\approx 2.7 \mu\text{m}$ to $\approx 210 \text{ nm}$ in size (Figure 3C). Smaller features enhance sensitivity by increasing surface area thereby improving exposure to the nucleic acid molecules. This facilitates microscale mass transfer of biomolecules and enables efficient drainage of the boundary layer of fluid through the pores within the dried blood matrix.^[27]

The described observations elucidate the individual consequences of drying and thermal lysis. Drying results in the formation of spherical structures both internally and externally, accompanied by smaller protrusions, whereas thermal lysis leads to the disintegration of these larger spherical structures due to increased water molecule movement facilitated by thermal energy. Interestingly, the spherical shapes appeared to remain largely intact even post-rupture, exhibiting minimal collapse or displacement (Figure S9B–D, Supporting Information). A summary of images depicting the dried blood matrix with and without additional thermal lysis can be found in Figures S10 and S11 (Supporting Information).

Quantifying the distribution of pore sizes is necessary to assess whether thermal lysis induces an increase in number of pores. Our BET and BJH analysis investigated the pore size distribution of dried blood matrix without and with additional thermal lysis steps (Figure 3D–G). Generally, the dried blood matrix displayed low porosity, $\approx 0.025 \text{ cm}^3 \text{ g}^{-1}$, with a structural composition resembling a combination of mesopores (2–50 nm) and macropores (exceeding 50 nm), featuring a non-crystalline, amorphous matrix (Figure 3E). This trait is anticipated to occur naturally, as we generate a novel substance through the amalgamation of various components like cells and proteins.

Following thermal lysis, a distinct alteration in the distribution was observed, indicating notable changes in the internal structure and porosity of the matrix, consequently influencing its permeability. A notable revelation is the augmentation in the number of smaller pores (shown as grey to black in Figure 3D,E) and the pore area (Figure 3F) induced by the thermal lysis process. The increased number of smaller pores is expected to alleviate structural dead ends, thereby reducing hydrodynamic resistance and the stagnation of reagents. Additionally, there was a ≈ 1.5 -fold increase in surface area, from 7 to $10.5 \text{ m}^2 \text{ g}^{-1}$ (Figure 3G), resulting in a higher probability of DNA exposure (Figure S12, Supporting Information). With these notable benefits, thermal lysis propels biphasic techniques toward increased reaction probability and increased sensitivity (Figure S2C, Supporting Information). Considering that our biphasic method modifies the structural properties of the material, these findings have implications for optimizing reagent delivery and improving the efficiency of molecular processes.

2.6. Analysis of Diffusion Coefficients

Characterizing the diffusion coefficient in dried blood can be important to understanding the overall performance of the system when molecules are introduced. To achieve this, we investigated the effective diffusion coefficients of molecules of different sizes within the dried blood matrix, both with and without the additional thermal lysis step. The size distribution of molecules present in the amplification master mix spans a wide range (Figure 4A), from sub-nanometer (Ångström) for ions and deoxyribonucleotide triphosphate (dNTPs), to a few nanometers for fluorescent reporters and primers, up to 10 nanometers for proteins and enzymes (e.g., DNA polymerase $\approx 94 \text{ kDa}$ and Bst Polymerase $\approx 97 \text{ kDa}$). To establish representative molecules for reference, we prepared two different sizes of green fluorescence molecules: 150 kDa (Stoke's radius of 8.5 nm) and 4 kDa

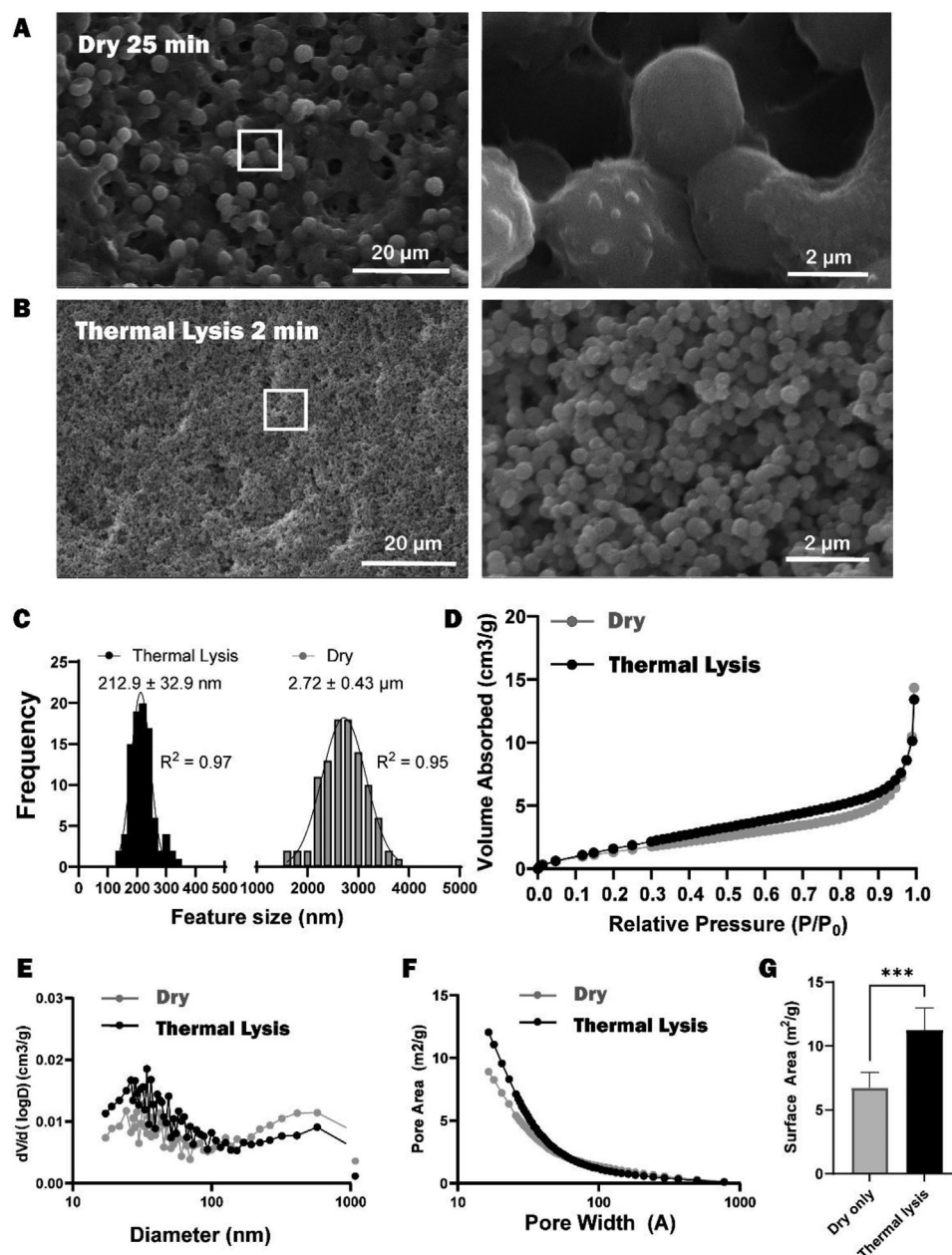


Figure 3. Material characterizations for improved delivery of master mix. SEM image of dried blood matrix A) before thermal lysis and B) after thermal lysis. The images to the right show an enlarged perspective of the specified area on the left, indicated by a white square. C) Feature size analysis D–G) BET-BJH analysis for dried sample and thermally lysed sample D) Absorbed volume of N₂ according to the pressure E) Pore size distribution F) Pore area distribution G) Surface area comparison ($n = 6$). Data are expressed in mean \pm SD. * $p < 0.05$, ** $p < 0.01$, *** $p < 0.001$.

(Stoke's radius of 1.4 nm size). We conducted FRAP measurements on dried blood matrices, both with and without thermal lysis using fluorescence microscopy (low porosity, larger features, Figure 4B Left, called "Dry") and with (high porosity, smaller features, Figure 4B Right, called "TL"). Following immersion of the dried blood matrix in a concentrated solution of green-fluorescence-tagged dextran molecules, a specific region of interest was subjected to photobleaching using a high-intensity laser. Subsequently, as these molecules diffused into the bleached area from the surrounding unbleached regions, the fluorescence in-

tensity within the bleached area gradually recuperated over time (Figure 4C) and was recorded (Figure 4D). By utilizing a fitting model for FRAP analysis (See Method section), the diffusion coefficient of the system was calculated. The findings indicated that the diffusion coefficients of both 4 and 15 kDa dextran molecules increased following thermal lysis (Figure 4E). For example, for 4 kDa molecules with an approximate size of 1.4 nm, it was estimated that their diffusion coefficient increased by 1.5 times after thermal lysis (from 38.4 to $57.4 \mu\text{m}^2 \text{s}^{-1}$).^[28] This enhancement in diffusion flux could potentially lead to a 16-minute reduc-

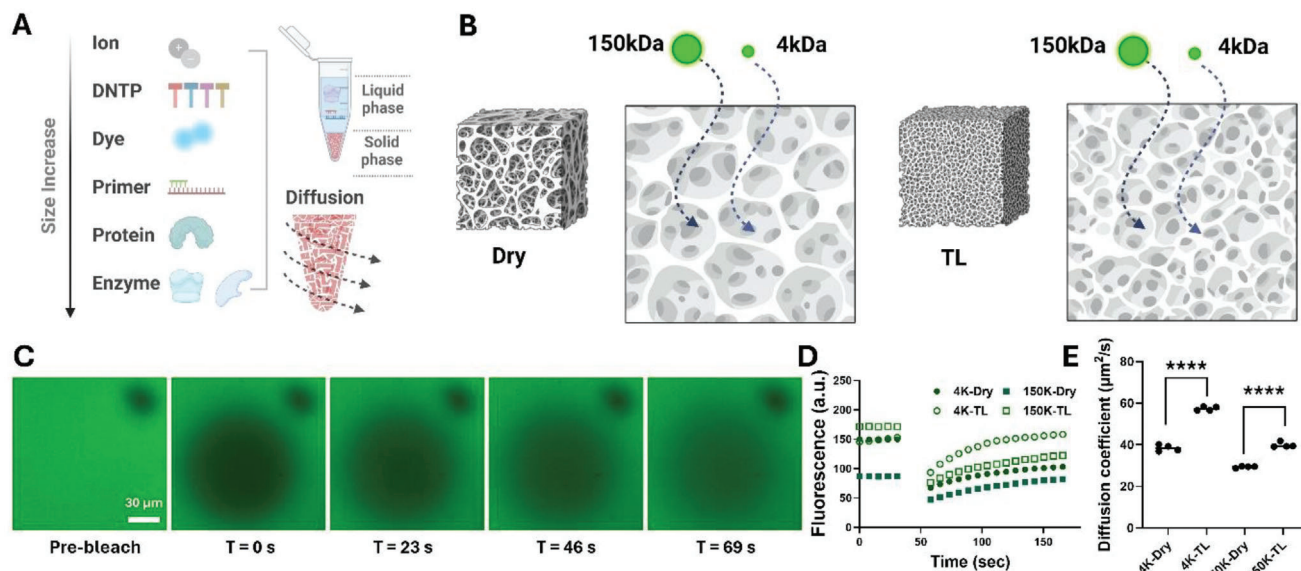


Figure 4. FRAP analysis A) Various molecules comprising the master mix with different sizes that require delivery B) A schematic representation illustrating the diffusion of two differently sized green fluorescence molecules into the dried and TL structures. C) Sequential images of FRAP captured over time, illustrating changes in fluorescence intensity within the region of interest. D) Quantification of measured fluorescence intensity E) Comparison of diffusion coefficient before and after thermal lysis. Data is presented individually for each instance, with a bar indicating the mean value. * $p < 0.05$, ** $p < 0.01$, *** $p < 0.001$, **** $p < 0.0001$.

tion in diffusion time for a 1 mm diffusion distance within the dried blood matrix. Considering that our biphasic-LAMP assay operates over an hour and the reaction mechanism is diffusion-limited, initiating the reaction 16 min earlier could have a significant impact on sensitivity.

Even though thermal lysis provides improved sensitivity, it appears to have an optimal duration range. For example, the rate of rupture for spherical particles seems to increase from 30 s to 2 min of thermal lysis, potentially leading to an increase in surface area (Figure S13A,B, Supporting Information). However, prolonged thermal lysis, such as for 5 min, appears to have the opposite effect, decreasing the porosity by compacting all void spaces with smaller features (Figure S13C, Supporting Information), thereby hindering the drainage of reagents through the matrix.

2.7. Assay Development using HBV Genomic DNA in Whole Blood

Leveraging our understanding of the material attributes of dried blood, we developed a biphasic HBV detection protocol with enhanced detection sensitivity (Figure 5A). Initially, we formulated a biphasic reaction for virus detection by incorporating spiked DNA into 4 μL of whole blood within standard PCR tubes (Figure 5B). Whole blood contained a desired concentration of HBV genomic DNA which was then dried for 25 min at 37 $^{\circ}\text{C}$. Given our findings that an additional thermal lysis step following blood drying enhances the porosity and increases surface area, we chose to employ the protocol involving both drying and thermal lysis as our control method. Briefly, we introduced HBV genomic DNA into whole blood, serially dilut-

ing it, and then dried the blood at 37 $^{\circ}\text{C}$ for 25 min. Following this, we introduced a buffer solution and subjected the biphasic matrix to thermal lysis at 95 $^{\circ}\text{C}$ for 2 min followed by a LAMP reaction. The normalized fluorescence data is available in Figure S14, (Supporting Information) and the threshold time corresponding to 20% of normalized fluorescence was plotted (Figure 5B). Our experimental results revealed that we could achieve single-copy sensitivity (1 copy/4 μL) without extraction and purification. For tubes containing a single copy of the sample, the expected fraction of amplifications observed was 3/8, in accordance with Poisson sampling statistics.^[29] No non-specific amplification was detected in non-target samples, including hepatitis C virus (HCV), methicillin-resistant *Staphylococcus aureus* (MRSA), *E. coli*, SARS-CoV-2, Zika, and negative controls (Figure S15, Supporting Information).

Subsequently, we examined larger volume reactions utilizing 100 μL of whole blood. In this approach, the assay was divided into three tubes, each containing 33 μL , and subjected to drying at 95 $^{\circ}\text{C}$ for 10 min, followed by thermal lysis (95 $^{\circ}\text{C}$ for 2 min) and biphasic LAMP reaction. A positive result was considered if any one of the three tubes exhibited an amplification reaction. Our results indicated that our assay successfully detected all replicates of 100 copies/100 μL , 6 out of 8 replicates of 10 copies/100 μL , and 4 out of 8 replicates of 1 copy/100 μL , thereby achieving zep-tomolar sensitivity (15 zM) with 100 μL of whole blood, without any observed non-specific reactions (Figure 5C). The increased sensitivity was made possible by the retrieval of all DNA without any loss during drying, in conjunction with our efficient reagent delivery approach, facilitating effective targeting of the DNA in the porous matrix. For further procedural details, please see the Methods section.

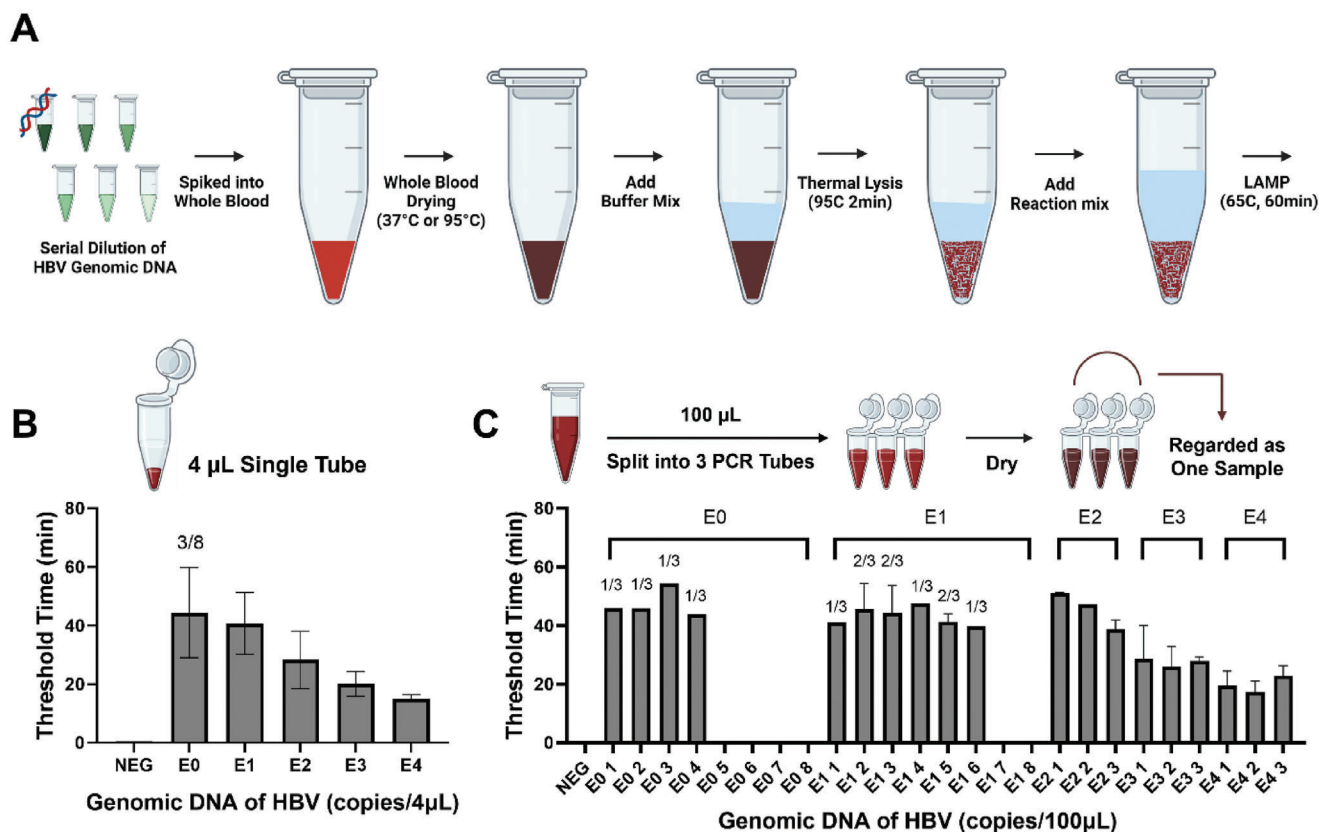


Figure 5. Biphase-LAMP assay development for the detection of HBV using genomic DNA in the whole blood. A) Protocol detailing the biphase LAMP procedure involving drying and thermal lysis B,C) Threshold time obtained from normalized fluorescence data with different concentrations of spiked genomic HBV DNA in B) 4 µL whole blood and C) 100 µL whole blood. Data are presented as mean ± SD ($n = 3$, unless otherwise indicated above the bar).

2.8. Comparison of the Current Gold Standard Technique and our Biphase HBV Assay

To assess the sensitivity of the biphase HBV reaction compared to the established gold standard method involving extraction and purification followed by PCR, we investigated the limit of detection of the conventional diagnostic approach. We employed active HBV virus spiked into whole blood to generate a starting sample in conjunction with extraction and purification kits. Two types of kits, namely Mini and Midi kits, which utilize 200 µL and 500 µL as a starting volume, respectively, were employed. Active HBV pathogen was spiked into the whole blood, and PCR was performed using the purified DNA obtained from each extraction and purification process.

Before delving into the impact of DNA loss during extraction and purification, we first validated the performance of the PCR assay used in this study by testing various concentrations of DNA spiked in water. Our PCR assay demonstrated a limit of detection reaching down to 1 genome copy per microliter sensitivity, exhibiting highly favorable linear regression and 0.9997 R-squared values (Figure S16, Supporting Information). This validation confirms that downstream PCR analysis can detect any concentration present in purified samples obtained from upstream extraction and purification procedures, thereby eliminating the potential for false negatives originating from the PCR assay itself.

The cycle threshold (C_T) values derived from whole blood samples spiked with active HBV pathogen are illustrated in Figure 6A. We tested various concentrations spiked in whole blood. As a result, the protocol utilizing the 200 µL sample volume exhibited limited sensitivity, with only 2 out of 8 replicates showing amplification for both 100 and 50 IU mL⁻¹ samples. No amplification was observed for concentrations lower than 25 IU mL⁻¹. In contrast, the protocol utilizing the 500 µL sample volume with the Midi kit demonstrated slightly improved sensitivity, particularly in the range of 100–50 IU mL⁻¹, where all 8 replicates for the 100 IU mL⁻¹ sample and 6 out of 8 replicates for the 50 IU mL⁻¹ sample exhibited amplification. However, a limited number of replicates showed amplification for the 25 and 10 IU mL⁻¹ samples.

The general trend reveals that the recovery rate decreases as the concentration of the target pathogen diminishes from 100 to 10 IU mL⁻¹, regardless of whether the 200 µL or 500 µL volume is used (Figure 6B). This emphasizes that the recovery rate depends on the total DNA amount in the starting material and may decline with very low concentrations, highlighting the necessity for a sample preparation protocol without DNA loss. In the case of plasma as the starting material, similar trends were observed, with 25 and 10 IU mL⁻¹ concentrations proving incompatible with the extraction and purification kit, as indicated by 0/8 replicates exhibiting amplification (Figure 6C). A consistent

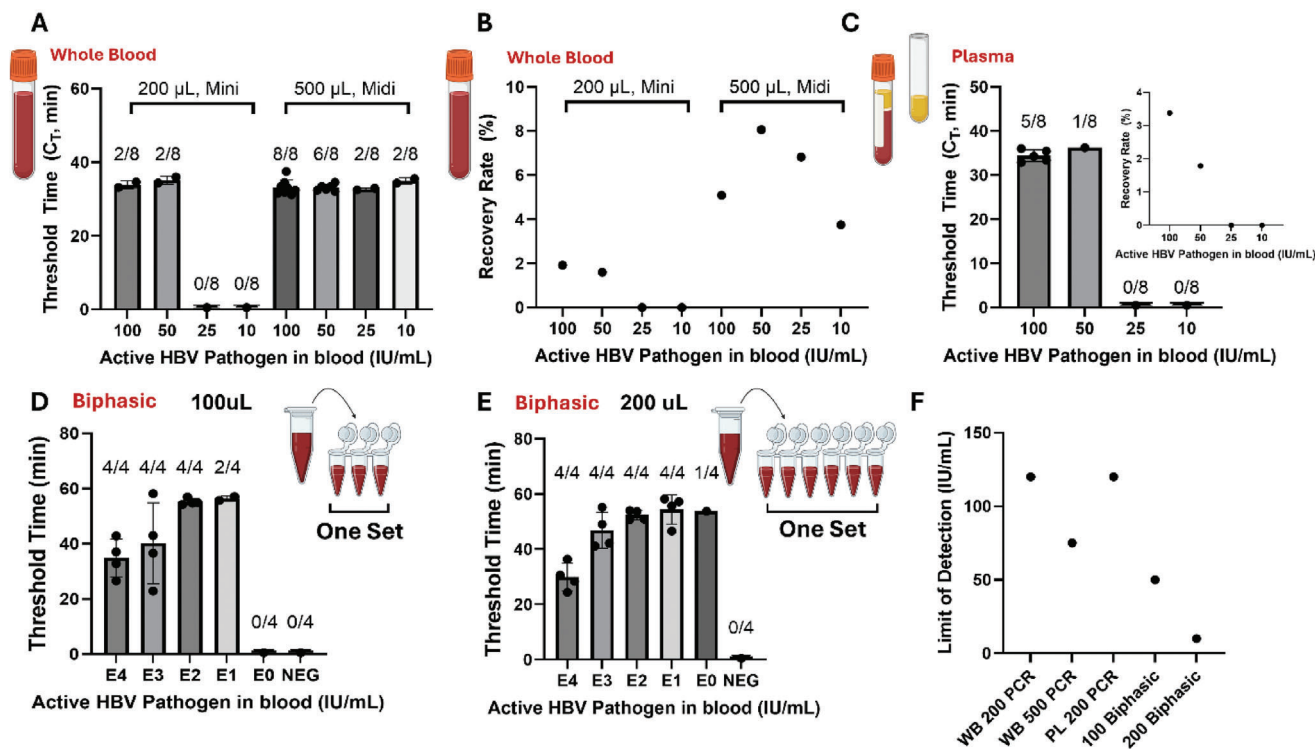


Figure 6. Comparison of the limit of detection between the current state-of-the-art method and the proposed biphasic LAMP assay using active HBV virus spiked in whole blood. A) Limit of detection of the PCR assay using extraction kits with 200 μL and 500 μL of whole blood format as starting materials B) Recovery rate of the extraction and purification kit C) Limit of detection of PCR assay using kits with 200 μL of plasma format as a starting material. Limit of detection of D) 100 μL and E) 200 μL biphasic LAMP assay. F) Summary of limit of detection for various assay types investigated. Data are presented as mean \pm SD, with the sample size (n) indicated above the bar.

trend of declining recovery rates corresponding to lower starting pathogen concentrations was observed, decreasing from $\approx 3.4\%$ to 1.8%, ultimately reaching 0%. Additional information can be found in Table S1 (Supporting Information).

On the contrary, our investigation into the sensitivity of the biphasic HBV reaction revealed a limit of detection as low as 10 IU mL^{-1} . Initially, we employed the protocol outlined in Figure 5C, wherein 100 μL of whole blood samples spiked with active HBV pathogen were split, and a biphasic LAMP reaction was conducted. We successfully detected 100 IU mL^{-1} with all 4 replicates and half of the 10 IU mL^{-1} samples (Figure 6D). Following this, to ensure comparable volume amounts to the conventional approach as starting material, we utilized 200 μL of whole blood samples, which were then split into 6 PCR tubes. Through this approach, we observed enhanced sensitivity, achieving a limit of detection of 10 IU mL^{-1} and even detecting amplification in 1 out of 4 replicates for the 1 IU mL^{-1} concentration reaction (Figure 6E; Figure S17, Supporting Information). Figure 6F provides a summary of the limit of detection for the investigated assays, with the 200 μL biphasic format demonstrating the highest sensitivity, with a limit of detection lower than 10 IU mL^{-1} .

Dried blood presents a complex matrix with distinctive attributes, and gaining insights into its material properties holds promise for advancements in blood diagnostics. The heterogeneous nature of the dried blood matrix leads to variable structures and porosity, influenced by factors such as drying temperature, humidity,^[30] surface chemistry,^[31] and starting material

properties^[32] such as the dilution ratio of whole blood. This poses challenges in understanding its underlying principles and complicates mass transfer within the system. Additionally, different starting materials can impact sensitivity, as demonstrated in previous studies where blood lysate obtained from partial red blood cell removal and bead vortexing for bacterial cell lysis exhibited similar detection limits to simply dried blood from blood lysate, without the need for thermal lysis.^[20]

The clinical distribution of HBV viral load spans various ranges: 10–30 IU mL^{-1} constitutes $\approx 20\%$ of cases of chronic hepatitis B, 30–100 IU mL^{-1} accounts for 13.5%, and 100–300 IU mL^{-1} makes up 17.8%, with a mean value of 776 IU $\text{mL}^{-1} \pm 42$.^[18] In instances of low-level viremia, HBV concentrations vary from 10–2000 IU, with reports indicating that 10–20 IU encompasses 45% of the population.^[19] This underscores the necessity for developing an assay of high sensitivity, capable of detecting concentrations as low as 10 IU mL^{-1} .

The current state-of-the-art technology such as Abbott Real-Time HBV, COBAS TaqMAN HBV Test, and Cephied Xpert, typically starts with EDTA plasma as a starting material (Table 1). This means that the centrifugation step should be the first procedure after drawing the blood from the patient. After that, complex instruments perform precise DNA extraction and purification. Even though PCR provides single-copy sensitivity, overall sensitivity is seriously compromised by a low recovery rate of upstream purification. For this reason, most of the automated machines begin with a substantial volume ranging from 0.5 mL to

Table 1. Comparison between biphasic approaches and existing technologies across multiple factors.

	Assay Type	Starting Material	Volume	Centrifuge	Ext and Pur	LOD [IU mL ⁻¹]	Assay Time [h]	POC Available	Reference
1	In-house Real-time PCR assay (this paper)	Whole blood	0.2 mL	No	Manual	> 100	2.5	No	This paper
2	In-house Real-time PCR assay (this paper)	Plasma	0.2 mL	Yes	Manual	> 100	2.5	No	This paper
3	Biphasic-HBV Diagnostic	Whole blood	0.2 mL	No	Manual	< 10	1.5	Yes	This paper
4	In-house Real-time PCR assay (reference)	Serum	0.2 mL	Yes	Manual	73 – 292	2.5	No	[33]
5	Abbott RealTime HBV	EDTA plasma or serum	0.2 mL	Yes	Automated (m2000sp)	15	2	No	Abbott
6	Roche COBAS Taqman HBV test	EDTA plasma or serum	0.2 mL	Yes	Automated (cobas 4800)	7.6	2	No	Roche
7	In-house Real-time PCR assay (this paper)	Whole blood	0.5 mL	No	Manual	50 – 100	2.5	No	This paper
8	Abbott RealTime HBV	EDTA plasma or serum	0.5 mL	Yes	Automated (m2000sp)	10	2	No	Abbott
9	Roche COBAS Taqman HBV test	EDTA plasma or serum	0.4 mL	Yes	Automated (cobas 4800)	4.4	2	No	Roche

1 mL to ensure enough total DNA amount is recovered. Actually, Abbott's HBV diagnostic has a different limit of detection depending on the sample volume (10 IU mL⁻¹ for 0.5 mL and 15 IU mL⁻¹ for 0.2 mL) with the serum or plasma as a starting material. In addition, diagnostic performance may vary depending on the skill level of the operator. When utilizing fully automated extraction machines like COBAS AmpliPrep with a 500 µL volume, the limit of detection decreases to 19 IU mL⁻¹, whereas with manual extraction using Qiagen with a 200 µL volume, the LOD is restricted to ≈200 IU mL⁻¹.^[33]

Biphasic HBV detection offers numerous key benefits over conventional diagnostic approaches, such as enhanced sensitivity, removal of extraction and purification steps, reduced assay time, elimination of sample transportation requirements, no centrifugation, and the opportunity for point-of-care testing. In the case of biphasic, 100 or 200 µL volume would be enough to achieve a target LOD. In the case of 200 µL volume protocol, 4/4 10 IU mL⁻¹ was detected and the sensitivity improved from 400 to 10 IU mL⁻¹ using the same LAMP primer but simply changing the sample preparation step from extraction and purification to biphasic format.^[34] The biphasic-HBV detection does not necessitate viral envelope rupture, significantly simplifying the process. Heating steps 1 and 2 alone suffice to lyse the virus and release the DNA contained within. Moreover, Biphasic LAMP offers the advantage of achieving results within 80 min (including 20 min for sample drying and thermal lysis, followed by up to a 60-minute reaction), whereas other methods require between 1.5 to 5 h. This timeframe does not account for the additional time required for sample transport to a centralized laboratory. For example, one of the challenges encountered in HBV DNA diagnostics arises in low-resource settings, where transportation of blood samples is necessary to begin with plasma or serum.^[35] Utilizing Biphasic-LAMP detection could offer a viable solution through enabling point-of-care testing, where the blood drawing site could facilitate HBV DNA detection from venous draw or finger prick. A comparable concept, dried blood spot, has been extensively employed for specimen collection and convenient delivery owing to its nucleic acid preservation attributes. However, its sensitivity is limited as it necessitates nucleic acid extraction from filter paper, where the paper itself contains amplification re-

action inhibitors.^[36] For instance, employing 50–70 µL of EDTA venous whole blood on Whatman 903 filter paper cards (Whatman, UK) has shown less than optimal sensitivity (> 1000 copies mL⁻¹), with ≈80% concordance with the gold standard testing.

The World Health Organization (WHO) estimates the cost per diagnostic for HBV to range between \$30 to \$200.^[37] An extraction kit combined with real-time turbidimetry is reported to cost \$14 for reagents, with instrumentation priced at ≈\$18 000.^[34] Even simpler extraction methods combined with end-point fluorescence detection are estimated to cost ≈\$8 for reagents and \$2750 for instrumentation.^[34] Our estimate using manual extraction and purification with PCR master mix incurs a minimal cost of \$5.64, but its sensitivity is limited to > 100 IU mL⁻¹, which may not be suitable given the HBV viral load distribution (Table S2, Supporting Information). This expense encompasses solely the extraction and purification kit alongside the PCR process itself. When starting with a 500 µL sample volume for improved sensitivity, the cost rises to \$16.8, as the Midi Kit is ≈3.5 times more expensive than the Mini Kit. On the contrary, biphasic LAMP reagents cost \$10 for a 100 µL format and \$20 for a 200 µL format (Table S2, Supporting Information). Since sample preparation begins directly from whole blood, no centrifugation is needed. The major advantage lies in the simplicity of the instrumentation required for biphasic LAMP, which involves a simple heater, without a function of temperature cycling, for all steps: heating, thermal lysis, and isothermal amplification (LAMP), significantly reducing instrumentation costs to a few hundred dollars.

3. Conclusion

The traditional approach to blood-based diagnostics for infectious diseases has remained largely unchanged, involving DNA extraction from crude samples followed by PCR using highly purified DNA. In this study, we present a revolutionary departure from this conventional method by directly delivering ample amplification reagents into the sample. Various techniques including SEM, BET and BJH pore analysis, and FRAP were employed to characterize the modified blood. A scientific comprehension of blood as a novel material was crucial in elucidating the significance of each biphasic step, which comprises drying and thermal

lysis. By immobilizing all inhibitor components and enhancing the diffusion speed of molecules within matrices, we have overcome the limitations of conventional diagnostics. Building upon this knowledge, we have devised an innovative solution to HBV diagnostics by combining novel blood drying with isothermal amplification techniques. Our biphasic-HBV diagnostic outperforms existing extraction and purification-based PCR technology in terms of sensitivity, time, cost, and portability.

4. Experimental Section

DNA and Virus: Quantitative synthetic DNA from the hepatitis B virus (HBV) was procured from ATCC (VR-3232SD) and was divided into appropriate volumes and concentrations before being stored at -80°C until required. Active HBV virus was obtained from ZeptoMetrix (0810031C) and was aliquoted into suitable volumes and concentrations before being stored at -80°C . Serial dilution was carried out using nuclease-free water with a 10 \times dilution factor to prepare aliquots.

Blood Preparation: Whole venous blood samples were acquired from the vendor BIOIVT, utilizing the HUMANWBK2- Human Whole Blood K2EDTA Gender Unspecified product. The blood was stored at 4°C on a sample rotisserie. For spiked whole blood samples, a similar 10 \times dilution of whole blood with the appropriate concentration was performed to create samples spiked with either HBV DNA or active HBV virus.

Biphasic Protocol: Heating Step 1 (Drying) and Heating Step 2 (Thermal lysis): Whole blood spiked with the desired concentration of target DNA or virus was transferred to standard PCR tubes with the appropriate volume. For the drying process, two different volumes were utilized: a small volume (4 μL) and a large volume (33 μL) format. The small volume method involved heating at 37°C for 25 min for drying, while the large volume method used 95°C for 10 min. Thermal lysis for both conditions was conducted at 95°C for 2 min. During thermal lysis, a buffer mix (LAMP master mix without enzyme and primer) was added to the dried blood matrix and incubated at 95°C .

SEM Analysis: The samples, either dried blood or thermally lysed, were fixed using 4% paraformaldehyde in PBS. After rinsing the samples with PBS, they were submerged in ethanol for the subsequent step. Following this, critical point drying was executed to remove moisture from the samples. Subsequently, the samples were coated with gold-palladium for improved imaging using the sputter instrument (Desk-II TSC). SEM imaging was conducted utilizing a Field-Emission Environmental Scanning Electron Microscope (FEI Quanta FEG 450 ESEM). The enumeration of individual spherical features was conducted on 10 SEM images using ImageJ software, and the results were graphically plotted.

BET and BJH Pore Size Distribution: The sample undergoes vacuum treatment on the SmartVac degasser, followed by heating to remove any lingering solvent or water trapped within the compound's pores. Next, the Micromeritics 3Flex Analyzer was utilized under the 77 K N2 adsorption condition to determine and calculate the Brunauer–Emmett–Teller (BET) surface area and Barrett–Joyner–Halenda (BJH) pore size distribution.

FRAP Analysis: Samples were treated with Fluorescein isothiocyanate (FITC)-dextran of varying sizes at a concentration of 20 mg mL^{-1} . Specifically, FITC-dextran with a molecular weight of 150 000 (FD150S) and with a molecular weight of 4000 (FD4) were obtained from Millipore Sigma for this purpose. These samples were stored at 4°C until required. Subsequently, they were loaded onto a confocal microscopy system (LSM 710, Zeiss) and examined using an excitation wavelength of 488 nm and an emission wavelength of 533 nm. For FRAP analysis, the internal software of the machine was utilized, and fluorescence data were recorded over time. A simple fitting formula of $D = r^2 / 4T$ (unit: $\mu\text{m}^2 \text{s}^{-1}$) was applied, where D represents the effective diffusion coefficient, r denotes the radius of the region of interest (or bleached spot), and T indicates the characteristic diffusion time calculated from software.

Immunostaining of Dried Blood Matrix: The samples underwent fixation using a solution containing 2% paraformaldehyde and 2.5% glu-

taraldehyde in PBS for 1 h, followed by thorough washing with PBS to remove excess fixative. Subsequently, they were blocked with a 2% BSA buffer for 30 min and washed again with PBS. The samples were then incubated overnight at 4°C with Anti-CD41 (ab308537) and Anti-Fibrin (ab4217) antibodies to target specific molecules.^[26] Finally, images were acquired using confocal laser microscopy (LSM 710, Zeiss) with a 488 nm laser for the green fluorescence channel and a 633 nm laser for the red fluorescence channel.

DNA Extraction and Purification: QIAamp DNA Blood Kits (51104 Mini and 51183 Midi, QIAGEN) were procured and utilized following the manufacturer's protocol. In the case of Mini kits, a 200 μL volume of whole blood spiked with varying concentrations of active HBV virus was employed. For plasma samples, whole blood spiked with various concentrations of active HBV virus was centrifuged for 10 min at 2000 g. After removing the 200 μL supernatant, it was utilized for subsequent extraction and purification procedures. A 500 μL volume of whole blood was used for Midi kits.

qPCR Analysis and Recovery Rate: The samples obtained after the final extraction and purification step were utilized for subsequent qPCR analysis. PowerTrack SYBR Green Master Mix (Thermo Fisher Scientific) was employed following the manufacturer's protocol. A 10 μL reaction format protocol was adopted, with 1 μL of sample volume used. Both forward and reverse primers were utilized at a concentration of 200 nM. A standard calibration curve was generated using HBV genomic DNA with concentrations ranging from 1 to 10^4 copies μL^{-1} through a 10-fold serial dilution. PCR reactions were conducted using the QuantStudio 3 system (Applied Biosciences), following the protocol provided by the PCR master mix supplier.

Utilizing the C_T value data and their linear interpolation, the recovery rate of extraction and purification across different spiked active HBV concentrations could be estimated. For HBV viral load conversion, 1 International Unit (IU) of HBV contains ≈ 5.26 copies of genomic DNA.^[38,39] Utilizing this conversion factor, along with the assumption of 100% sensitivity for PCR, the recovery rate of the extraction and purification process could be computed. For instance, a sample with a concentration of 100 IU mL^{-1} statistically contains 20 IU in 200 μL starting volume, corresponding to 112 copies of total HBV DNA. To be specific, with an average C_T value of 33.886 obtained from two amplified replicates, signifying the detection of 2.14 copies through interpolation, the recovery rate of the extraction and purification kit could be determined as $2.14 / 112 \times 100$, as presented in Figure 6B.

Primer Sequences: All primer sequences for the PCR and LAMP reactions were synthesized by Integrated DNA Technologies (IDT). PCR primer targeting the S region of HBV was adopted from the reference.^[40] LAMP primers were adopted from the following reference.^[34] Their individual sequence can be found in Table S3 (Supporting Information).

LAMP Reactions: For biphasic LAMP reactions, the LAMP master mix could be categorized into two components: buffer mix and reaction mix. The buffer mix comprises several constituents, including 1 \times isothermal amplification buffer (from New England Biolabs), 1.025 mmol L^{-1} of each deoxyribonucleoside triphosphate (dNTP), 4 mmol L^{-1} of MgSO_4 (from New England Biolabs), 0.29 mol L^{-1} of Betaine (from Sigma-Aldrich), 1 mg mL^{-1} of BSA (from New England Biolabs), and 1 \times EvaGreen (from Biotium), a double-stranded DNA intercalating dye. The reaction mix encompasses both the buffer mix and primer and polymerase components. Specifically, the reaction mix comprises 0.15 μM of F3 and B3, 1.17 μM of FIP and BIP, and 0.59 μM of LoopF and LoopB primers, along with 0.47 U μL^{-1} of Bst 2.0 WarmStart DNA Polymerase (from New England Biolabs). In a sample reaction volume of 4 μL , 4 μL of buffer mix was utilized, followed by the addition of 12 μL of reaction mix after thermal lysis. For a 33 μL sample volume format, the total master mix volume was 96 μL , comprising 72 μL of buffer mix and 24 μL of reaction mix. LAMP reactions were conducted in the QuantStudio 3 system (from Applied Biosciences) at a constant temperature of 65°C for 60 min. Fluorescence data were measured and recorded every minute. Raw fluorescence data were normalized, and the amplification threshold time was determined by identifying the point at which 20% of the normalized fluorescence threshold was achieved.

Statistical Analysis: The data were displayed either as the mean \pm SEM or as the mean with individual data points. Statistical analysis was performed using a two-tailed unpaired t-test with GraphPad Prism (version 10.2.3). A *p*-value of <0.05 was regarded as statistically significant.

Supporting Information

Supporting Information is available from the Wiley Online Library or from the author.

Acknowledgements

R.B. and E.V. acknowledge support from the Jump ARCHES (Applied Research through Community Health through Engineering and Simulation) endowment through the Health Care Engineering Systems Center at UIUC and OSF. This work was supported, in part, by the Dynamic Research Enterprise for Multidisciplinary Engineering Sciences (DREMES) Center funded by the Zhejiang University of Illinois ZJUI Joint Institute. The authors thank the staff at the Holonyak Micro and Nanotechnology Laboratory at UIUC for facilitating the research and the funding from the University of Illinois.

Conflict of Interest

The authors declare no conflict of interest.

Author Contributions

J.L., E.V., H.K., and R.B. designed the research; J.L., J.H., H.M., and M.W., performed the research. J.H. assisted with FRAP analysis. H.M. assisted with Immunostaining analysis. H.M. and C.K. assisted with data interpretation and analysis. R.B. supervised research. All authors assisted with manuscript editing.

Data Availability Statement

The data that support the findings of this study are available from the corresponding author upon reasonable request.

Keywords

direct detection from whole blood, DNA amplifications, dried blood matrix, hepatitis B virus, material characterization, point-of-care diagnostics, purification-free amplifications

Received: July 8, 2024

Revised: July 16, 2024

Published online:

- [1] M. Karlikow, S. J. R. da Silva, Y. Guo, S. Cicek, L. Krokovsky, P. Homme, Y. Xiong, T. Xu, M. A. Calderón-Peláez, S. Camacho-Ortega, D. Ma, J. J. F. de Magalhães, B. N. R. F. Souza, D. G. de Albuquerque Cabral, K. Jaenes, P. Sutyrina, T. Ferrante, A. D. Benitez, V. Nipaz, P. Ponce, D. G. Rackus, J. J. Collins, M. Paiva, J. E. Castellanos, V. Cevallos, A. A. Green, C. Ayres, L. Pena, K. Pardee, *Nat. Biomed. Eng.* **2022**, 6, 246.

- [2] M. Sinha, J. Jupe, H. Mack, T. P. Coleman, S. M. Lawrence, S. I. Fraley, in *Emerging technologies for molecular diagnosis of sepsis*, American Society for Microbiology, USA **2018**.
- [3] T. Demeke, G. R. Jenkins, *Anal. Bioanal. Chem.* **1977**, 2010, 396.
- [4] M. N. Emaus, M. Varona, D. R. Eitzmann, S. A. Hsieh, V. R. Zeger, J. L. Anderson, *TrAC – Trends Anal. Chem.* **2020**, 130, 115985.
- [5] N. Garg, F. J. Ahmad, S. Kar, *Curr Res Microb Sci.* **2022**, 3, 100120.
- [6] I. M. Lobato, C. K. O'Sullivan, *TrAC – Trends Anal. Chem.* **2018**, 98, 19.
- [7] P. E. Vandeventer, K. M. Weigel, J. Salazar, B. Erwin, B. Irvine, R. Doebler, A. Nadim, G. A. Cangelosi, A. Niemz, *J Clin Microbiol.* **2011**, 49, 2533.
- [8] M. Kang, E. Jeong, J. Y. Kim, S. A. Yun, M. A. Jang, J. H. Jang, T. Y. Kim, H. J. Huh, N. Y. Lee, *Sci. Rep.* **2023**, 13, 20364.
- [9] D. Cai, O. Behrmann, F. Hufert, G. Dame, G. Urban, in *Direct DNA and RNA detection from large volumes of whole human blood*, Springer US, USA **2018**.
- [10] I. A. Nanayakkara, W. Cao, I. M. White, *Anal. Chem.* **2017**, 89, 3773.
- [11] C. Katevatis, A. Fan, C. M. Klapperich, *PLoS One.* **2017**, 12, e0176848.
- [12] J. Lim, R. Stavins, V. Kindratenko, J. Baek, L. Wang, K. White, J. Kumar, E. Valera, W. P. King, R. Bashir, *Lab Chip.* **2022**, 22, 1297.
- [13] I. Smyrlaki, M. Ekman, A. Lentini, N. Rufino de Sousa, N. Papanicolaou, M. Vondracek, J. Aarum, H. Safari, S. Muradrasoli, A. G. Rothfuchs, J. Albert, B. Högberg, B. Reinius, *Nat. Commun.* **2020**, 11, 4812.
- [14] L. B. Reller, M. P. Weinstein, G. A. Storch, *Clin. Infect. Dis.* **2000**, 31, 1209.
- [15] Y. Bu, H. Huang, G. Zhou, *Anal. Biochem.* **2008**, 375, 370.
- [16] C. M. Buchanan, R. L. Wood, T. R. Hoj, M. Alizadeh, C. G. Bledsoe, M. E. Wood, D. S. McClellan, R. Blanco, C. L. Hickey, T. V. Ravsten, G. A. Hussein, R. A. Robison, W. G. Pitt, *J Microbiol Methods.* **2017**, 139, 48.
- [17] A. Ganguli, A. Mostafa, J. Berger, J. Lim, E. Araud, J. Baek, S. A. Stewart De Ramirez, A. Baltaji, K. Roth, M. Aamir, S. Aedma, M. Mady, P. Mahajan, S. Sathe, M. Johnson, K. White, J. Kumar, E. Valera, R. Bashir, *Anal. Chem.* **2021**, 93, 7797.
- [18] F. Mathai, M. Otieno Ngayo, S. Muturi Karanja, A. Kalebi, R. Lihana, *Arch. Clin. Infect. Dis.* **2017**, 12, 13306.
- [19] J. Han, Y. Guo, X. Zhang, Y. Zhang, J. Sun, J. He, R. Mao, Y. Huang, J. Zhang, *Turkish J. Gastroenterol.* **2023**, 34, 53.
- [20] A. Ganguli, J. Lim, A. Mostafa, C. Saavedra, A. Rayabharam, N. R. Aluru, M. Wester, K. C. White, J. Kumar, R. McGuffin, A. Frederick, E. Valera, R. Bashir, *Proc. Natl. Acad. Sci. USA.* **2022**, e2209607119.
- [21] J. Lim, S. Zhou, J. Baek, A. Y. Kim, E. Valera, J. Sweedler, R. Bashir, *Small.* **2023**, 20, 2307959.
- [22] M. Guvenir, A. Arikan, *Polish J. Microbiol.* **2020**, 69, 391.
- [23] L. M. Villar, H. M. Cruz, J. R. Barbosa, C. S. Bezerra, M. M. Portilho, L. de P. Scalioni, *World J Virol.* **2015**, 4, 323.
- [24] A. W. Gani, W. Wei, R. Z. Shi, E. Ng, M. Nguyen, M. S. Chua, S. So, S. X. Wang, *Sci. Rep.* **2019**, 9, 15615.
- [25] Y. Shimakawa, G. Ndow, A. Kaneko, K. Aoyagi, M. Lemoine, Y. Tanaka, T. Cerceau, A. Ceesay, J. Perpétue Vincent, T. Watanabe, M. Baba, B. Sanneh, I. Baldeh, R. Njie, U. D'Alessandro, M. Mendy, I. Chemin, M. R. Thursz, *Clin. Gastroenterol. Hepatol.* **2023**, 21, 1943.
- [26] S. H. Jung, B. H. Jang, S. Kwon, S. J. Park, T. E. Park, J. H. Kang, *Adv. Mater.* **2023**, 35, 2300091.
- [27] P. Zhang, X. Zhou, M. He, Y. Shang, A. L. Tetlow, A. K. Godwin, Y. Zeng, *Nat. Biomed. Eng.* **2019**, 3, 438.
- [28] A. Bläßle, G. Soh, T. Braun, D. Mörsdorf, H. Preiß, B. M. Jordan, P. Müller, *Nat. Commun.* **2018**, 9, 1582.
- [29] R. A. Lee, H. De Puig, P. Q. Nguyen, N. M. Angenent-Mari, N. M. Donghia, J. P. McGee, J. D. Dvorin, C. M. Klapperich, N. R. Pollock, J. J. Collins, *Proc. Natl. Acad. Sci. USA.* **2020**, 117, 25722.
- [30] N. Laan, F. Smith, C. Nicloux, D. Brutin, *Forensic Sci Int.* **2016**, 267, 104.

- [31] B. S. Frey, D. E. Damon, D. M. Allen, J. Baker, S. Asamoah, A. K. Badu-Tawiah, *Analyst*. **2021**, 146, 6780.
- [32] A. Pal, A. Gope, G. Iannacchione, *Biomolecules*. **2021**, 11, 231.
- [33] D. Kania, L. Ottomani, N. Meda, M. Peries, P. Dujols, K. Bolloré, W. Rénier, J. Viljoen, J. Ducos, P. Van de Perre, E. Tuaillon, *J. Virol. Methods*. **2014**, 201, 24.
- [34] J. Vanhomwegen, A. Kwasiborski, A. Diop, L. Boizeau, D. Hoinard, M. Vray, R. Bercion, B. Ndiaye, A. Dublineau, S. Michiyuki, J. C. Manuguerra, V. Sauvage, D. Candotti, A. Seck, S. Laperche, Y. Shimakawa, *Clin. Microbiol. Infect.* **2021**, 27, 1858e9.
- [35] A. Kramvis, K. M. Chang, M. Dandri, P. Farci, D. Glebe, J. Hu, H. L. A. Janssen, D. T. Y. Lau, C. Penicaud, T. Pollicino, B. Testoni, F. Van Bömmel, O. Andrisani, M. Beumont-Mauviel, T. M. Block, H. L. Y. Chan, G. A. Cloherty, W. E. Delaney, A. M. Geretti, A. Gehring, K. Jackson, O. Lenz, M. K. Maini, V. Miller, U. Protzer, J. C. Yang, M. F. Yuen, F. Zoulim, P. A. Revill, *Nat. Rev. Gastroenterol. Hepatol.* **2022**, 19, 727.
- [36] E. Tuaillon, D. Kania, A. Pisoni, K. Bolloré, F. Taieb, E. N. Ontsira Ngoyi, R. Schaub, J. C. Plantier, A. Makinson, P. Van de Perre, *Front. Microbiol.* **2020**, 11, 373.
- [37] WHO Guidelines on hepatitis B and C testing, **66**, **2017**.
- [38] C. M. Chu, Y. C. Chen, D. I. Tai, Y. F. Liaw, *Clin. Gastroenterol. Hepatol.* **2010**, 8, 535.
- [39] C. Ronsin, A. Pillet, C. Bali, G. A. Denoyel, *J. Clin. Microbiol.* **2006**, 44, 1390.
- [40] C. Liu, L. Chang, T. Jia, F. Guo, L. Zhang, H. Ji, J. Zhao, L. Wang, *Virology*. **2017**, 14, 1.